

Received March 15, 2019, accepted April 18, 2019, date of publication April 25, 2019, date of current version May 13, 2019.

Digital Object Identifier 10.1109/ACCESS.2019.2913278

High-Performance and Ultra-Broadband Metamaterial Absorber Based on Mixed Absorption Mechanisms

CAN-YU WANG¹, JIAN-GANG LIANG¹, TONG CAI¹, HAI-PENG LI¹,
WEN-YE JI¹, QING ZHANG², AND CHENG-WU ZHANG²

¹Air and Missile Defense College, Air force Engineering University, Xi'an 710051, China

²The Research Institute for Special Structures of Aeronautical Composite ACICA, The Aeronautical Science Key Lab for High Performance Electromagnetic Windows, Ji'nan 250023, China

Corresponding authors: Jian-Gang Liang (cat_liang@163.com) and Tong Cai (caitong326@sina.cn)

This work was supported in part by the National Natural Science Foundation of China (NSFC) under Grant 61871394 and Grant 61701572, and in part by the Aeronautical Science Foundation of China (ASFC) under Grant 20151896014.

ABSTRACT Perfect absorbers are highly desirable in many military applications, such as radar cross section (RCS) reduction, cloaking devices, and also sensor detectors; however, most approaches (such as wedge and pyramidal absorbers, multi-resonant absorbers) intrinsically suffer from very large size at low-frequency domain, limited bandwidth, as well as low absorption ratio issues. In this paper, we solve these issues via combining the Huygens metasurface and three-layers slab impedance metasurface, with the former satisfying the novel impedance matching theory and the latter exhibiting multi-resonant property and optimized conductivities, which achieve *high-efficiency* absorption at lower frequency range (1–3 GHz) and higher frequency region (3–18 GHz), respectively. To demonstrate our concept, we design/fabricate a realistic metasurface absorber working in the microwave region, and perform experiments to demonstrate that it can achieve an *ultra-broadband* (1–18 GHz) performance with absorption rate better than 75%. The numerical simulations are in good agreements with experiments, indicating that the absorption efficiency can be further pushed to 92% within the whole working band by optimizing our designs. More importantly, our device is insensitive for different polarizations and oblique incidences. Our findings can stimulate the realizations of ultra-broadband meta-devices, particularly can enhance the cloaking technology relying on high-efficiency absorption.

INDEX TERMS Ultra-broadband absorption, mixed absorption mechanisms, high absorption rate, polarization insensitive.

I. INTRODUCTION

Electromagnetic (EM) stealth technology is believed to be a key to improve the penetration ability of weapon systems in modern warfare. Perfect absorber is demonstrated as an important method to realize the EM stealth [1]. A vital scientific issue is that, how to achieve perfect absorption within an *ultra-broadband* by using one single device with very *high absorption efficiency*?

Conventional absorbers are constructed by natural materials (e.g. wedge absorbers or ferrite [2], [3]), which are electrically large, configuration complex as well as expensive cost, being inconvenient for integration applications.

The associate editor coordinating the review of this manuscript and approving it for publication was Ildiko Peter.

Metamaterials, especially its planar version, metasurfaces (planar inhomogeneous metamaterials composed of carefully selected “meta-atoms” with specific EM responses [4]), have become a field of intense research activities with remarkable achievements, including invisibility cloaks [5], [6], super-lens [7], [8], planar holograms [9]–[11] as well as perfect absorbers [1], [12]–[31]. Since they demonstrate strong electronic/magnetic resonances at particular frequencies, metamaterial absorbers have been realized at single band, dual band and multi-band [12]–[15]. Moreover, the operating frequencies have been extended from microwave to Terahertz and visible ranges [1], [13]–[20], [23], [27]–[30]. However, highly effective absorption at particular frequencies is always accompanied with the narrow bandwidth, which is the inherent property of resonant structures. Recently, many effects

have been devoted to broadening the bandwidth of metamaterial absorbers, such as incorporating varied geometries in one meta-atom [13], [14], [19], [20], [22], [30], using some meta-atoms with different sizes [21], [23], loading lumped elements [21], [24]–[26], employing fractal patterns [26], [27] and other methods [28]–[31]. However, either the realized absorption frequency window is narrow, or the absorption ratio is very low, or the size is quite large at low frequency, which limits their further applications.

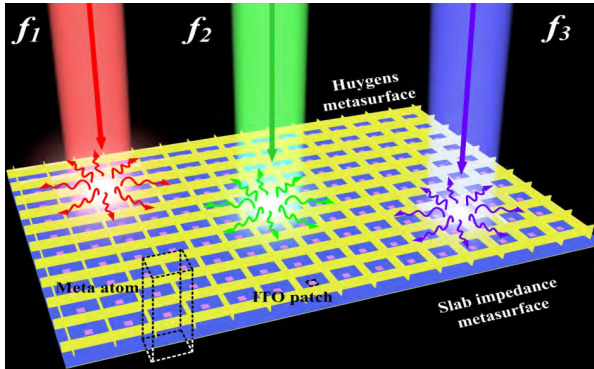


FIGURE 1. Schematics and working principles of the proposed absorber. Our system is composed of the Huygens metasurface at the upper part and the slab impedance metasurface at the lower part. The electromagnetic energy at low frequency f_1 (red part representing frequency of f_1) is mainly absorbed by the Huygens metasurface, while the energy at high frequency range (green and blue part representing frequencies of f_2 and f_3) is absorbed by the slab impedance metasurface.

In this paper, we propose a new strategy to achieve *ultra-broadband* (1 GHz–18 GHz) and *perfect* (higher than 90%) absorber at a *subwavelength* size by using mixed absorption mechanisms. Schematically shown in Fig. 1, the novel impedance matching theory realized by Huygens metasurface [32] and the multi-resonant theory achieved by the slab impedance metasurface, are built to broaden the bandwidth at lower and higher frequency bands, respectively. As a proof of concept, we fabricate a microwave sample to experimentally demonstrate our design. The results show that the combination of Huygens metasurface and the slab impedance metasurface exhibit high-performance absorption (> 90%) covering frequency window of better than 1–18 GHz. Our strategy provides practical approaches to design broadband absorber at other frequency domains or tailor the absorption rate by using different theories.

II. MIXED MECHANISMS AND META-ATOM DESIGN

We first discuss the mixed mechanisms of high-performance absorption. Here, the ultra-broadband absorption mechanisms include two components. For the low frequency range, we propose a novel impedance matching theory, which is inspired by the perfectly matched layer (PML) theory. As shown in Fig. 2(a), for a reflective system with a thin copper layer (0.036 mm) on the ground layer, the key step of achieving perfect absorption is to realize impedance matching between free space ($\eta_0 = 377\Omega$) and the copper layer ($\eta = 0\Omega$). Fig. 2(b) depicts the impedance

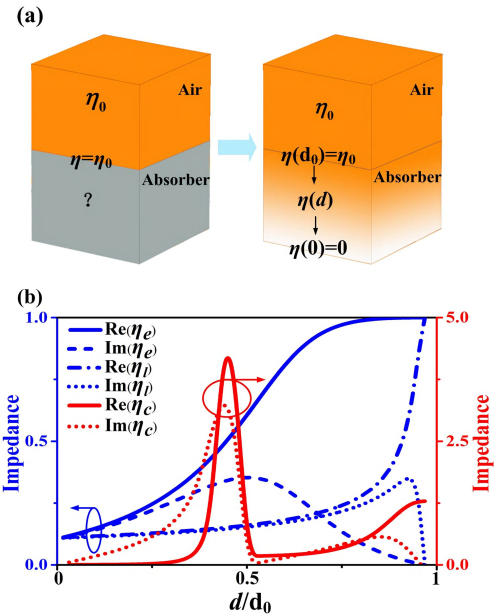


FIGURE 2. Absorption mechanism of the novel impedance matching theory. (a) Effective model of traditional resonant absorber on the left and the novel model with gradient-impedance property. (b) Effective wave impedance curves inside the structures for the conventional resonant structures and novel model with gradient-impedance property. Blue lines denote the calculated real and imaginary parts of impedance as σ changes with exponential and linear relationships (the subscript of η denotes the change relationship of σ), while the red lines show the impedance of the conventional resonant structures. The calculated impedance is normalized to that of free space.

curves inside the structures for the conventional resonant model and the gradient-impedance model. The impedance curve changes sharply for the conventional metamaterial absorbers because of the resonances of the structures and only particular frequency can fulfill the impedance matching condition, which is the original reason of the narrow bands [1], [12]–[15], [19]–[27]. In our proposed gradient-impedance model, we divide the structure into a multi-layer system. The mechanism of wideband absorption is to study the rule of impedance distribution on each layer. According to the PML theory [33], the impedance on each layer can be calculated by the formula

$$\eta(d) = \left[\frac{\mu_0 + \sigma_m(d)/(j\omega)}{\varepsilon_0 + \sigma(d)/(j\omega)} \right]^{1/2} \tag{1}$$

Here, σ_m denotes the magnetic-conductivity excited by the magnetic currents, μ_0 and ε_0 being the permeability and permittivity in free space, respectively. Here, we set $\sigma_m = 0$ for the unexcited magnetic currents. At the interface between two adjacent layers, the conductivity can be obtained according to the boundary condition of $\sigma_{(l)} = \sigma_{(l+1)}$. Either for a linear or exponential change of the $\sigma(d)$, the impedance curves change gently from 0 to η_0 , as shown in Fig. 2(b). More importantly, the real part of the impedance avoids the sharp peak resulting from the strong resonance (demonstrated by the red line in Fig. 2(b)), which is very essential to achieve wideband absorption. At the high frequency range, we enhance the absorption efficiency and extend the

bandwidth by using two factors: tuning the conductivity of the material (σ) and combining several absorption bands. As discussed in Ref. [34], σ can obviously affect the absorption rate whereas have minor effects on the resonance, while the resonant structures can affect the operating frequencies, which is demonstrated effectively in Fig. 3.

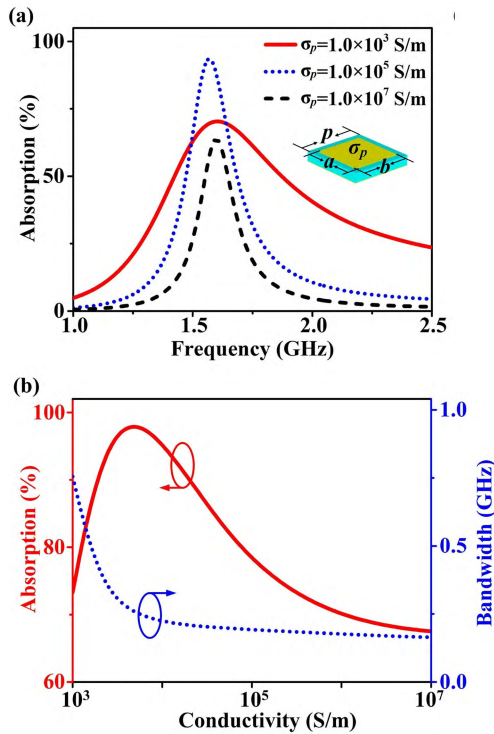


FIGURE 3. Affection of conductivity to absorption performance. (a) Absorption ratios of patch resonator absorber changing against conductivity (σ_p) of the patch, and inset shows the meta-atom schematic. The periodicity of the meta-atom is $p = 40$ mm, the patch size is $a \times b = 38 \times 38$ mm. (b) Maximum absorption ratio and full width at half-maximum (FWHM) absorption bandwidth under different conductivity.

In order to analyze how the conductivity influences the absorption ratio and bandwidth, we designed a simple patch resonator absorber shown in the inset of Fig. 3(a). The basic meta-atom is a sandwich structure, consisting of a metallic patch resonator with size $a \times b = 38 \times 38$ mm and a continuous metal sheet, separated by a 3 mm thick FR4 ($\epsilon_r = 4.3 + 0.025i$) spacer. Fig. 3(a) plots the absorption spectrum of the absorber at three representative values of conductivity. We note that the maximum absorption ratio at resonance frequency can be significantly affected by the values of conductivity σ_p . While the resonance frequency almost keeps constant. The absorption ratio reaches maximum at $\sigma_p = 8 \times 10^3$ S/m, see the absorption peak curves in Fig. 3(b). The maximum absorption ratio increases when σ_p is less than 8×10^3 S/m, while decreases as σ_p is larger than 8×10^3 S/m. Moreover, we can see clearly that the full width at half-maximum (FWHM) absorption bandwidth, can be dramatically enhanced as σ_p decreases, see the bandwidth curve in Fig. 3(b). Therefore, we can make a balance between

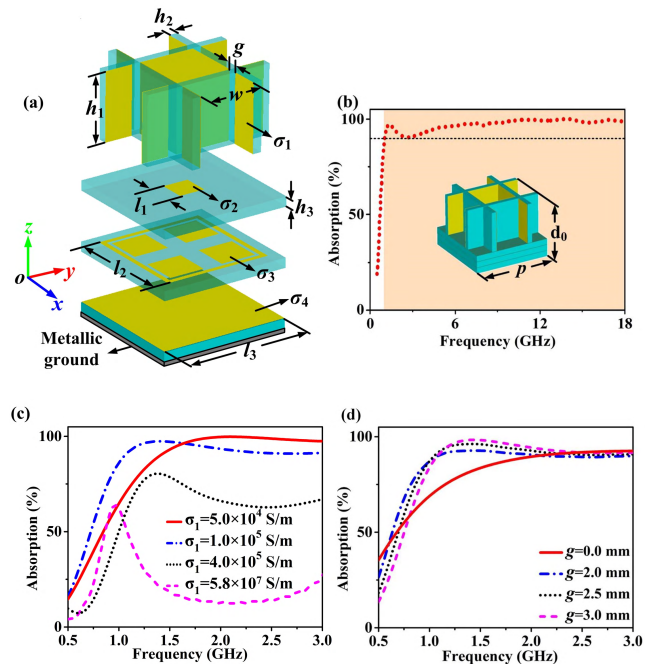


FIGURE 4. Design of the ultra-broadband microwave absorber. (a) Schematic of the proposed meta-atom. The geometrical parameters are listed as: $h_1 = 21$ mm, $g = h_2 = 2.5$ mm, $w = 20$ mm, $h_3 = 3$ mm, $l_1 = 8$ mm, $l_2 = 35$ mm, $l_3 = 39$ mm, $\sigma_2 = 6.7 \times 10^4$ S/m, $\sigma_3 = 2.0 \times 10^5$ S/m, $\sigma_4 = 2.0 \times 10^5$ S/m. (b) FDTD calculated reflection coefficient against frequency of our absorber. Inset to (b) shows the schematic of the meta-atom with $p = 40$ mm and $d_0 = 31.6$ mm. The absorption ratios for the Huygens metasurface at low frequency range changing against (c) the conductivity σ_1 of ITO films and (d) gap widths.

the absorption ratio and the bandwidth by adjusting the conductivity carefully.

We next design a realistic structure by using the proposed mixed mechanisms. As schematically depicted in Fig. 4(a), our structure consists of the upper Huygens metasurface and the lower three-layer slab impedance metasurface. The Huygens metasurface is designed to realize the gradient-impedance property. And for the Huygens metasurface, two vertical cross-patches are supported by FR4 substrate with thickness of $h_2 = 2.5$ mm. Each patch, loaded with two gaps, is covered by a thin indium tin oxide (ITO) film with $\sigma_1 = 2 \times 10^5$ S/m. The conductivity of the ITO and the size of the gaps are optimized to realize a good impedance matching property at the low frequency range (1-3 GHz). The absorption ratio can be estimated by the equation of $A = 1 - |S_{11}|^2 - |S_{21}|^2$ [12]. Fig. 4(c) depicts the absorption curves varying against the conductivity (σ_1) of the ITO. We can see that the absorption ratio can be significantly enhanced as σ_1 decreased. For the copper-covering condition ($\sigma_1 = 5.8 \times 10^7$ S/m), the Huygens metasurface can only realize an absorption of less than 65%, while the absorption can increase to more than 90% when σ_1 decreased. Moreover, the absorption bandwidth, ordered by 90% absorption ratio, can be affected largely by the values of σ_1 . The width of the dual gaps (g) can affect the operating frequencies, as shown in Fig. 4(d). There is no absorption peak at low frequency

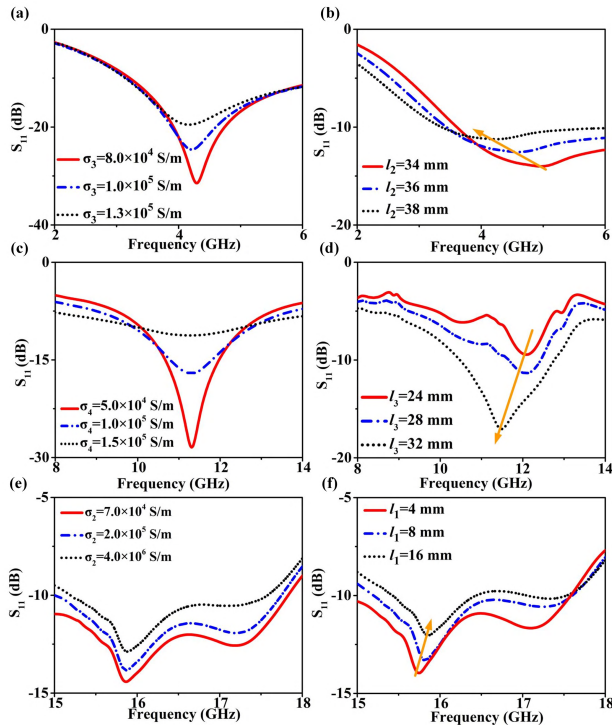


FIGURE 5. Process of parameters adjustment in slab impedance metasurface. The reflection coefficients at first absorption band for the slab impedance metasurface varying against (a) conductivity σ_3 on the second layer and (b) the square ring size l_2 , (c) and (d) reflection coefficients at the second absorption band for conductivity σ_4 on the third layer and patch size l_3 . (e) and (f), reflection coefficients varying against conductivity on the top layer σ_2 and patch size l_1 at third absorption band.

range without gaps ($g = 0$), while the operating frequency shift upwards as g increases. Therefore, we can obtain a wide absorption bandwidth as well as a desirable absorption ratio at low frequency range by changing σ_1 and g .

The three-layer slab impedance metasurface consists of three patch resonators separated by three substrates. The continuous metal sheet on the ground plane can naturally reflect all incoming wave back [1], [13]–[27]. The slab impedance metasurface is applied to achieve high-efficiency absorption at high frequency range (3-18 GHz). In fact, three absorption bands, realized by the patch geometries on different layers, are combined together to cover the high frequency range. For the first absorption band, Figs. 5(a) and 5(b) illustrate the absorption performances varying against the conductivity of ITO film on the second layer (σ_3) and the ITO square ring size (l_2). It is obvious that the absorption ratio is enhanced as σ_3 decreased, while the operating frequency declines with the increase of l_2 . Fig. 6(f) indicates current distribution at first absorption band. And for the second absorption band, the resonance is induced by the structures on the second and third layers, which is demonstrated by the current-distributions shown in Fig. 6(g). The conductivity σ_4 and the parameter l_3 affect the absorption ratio and the operating frequency, respectively, which is verified by the absorption spectra shown in Figs. 5(c) and (d). At the third

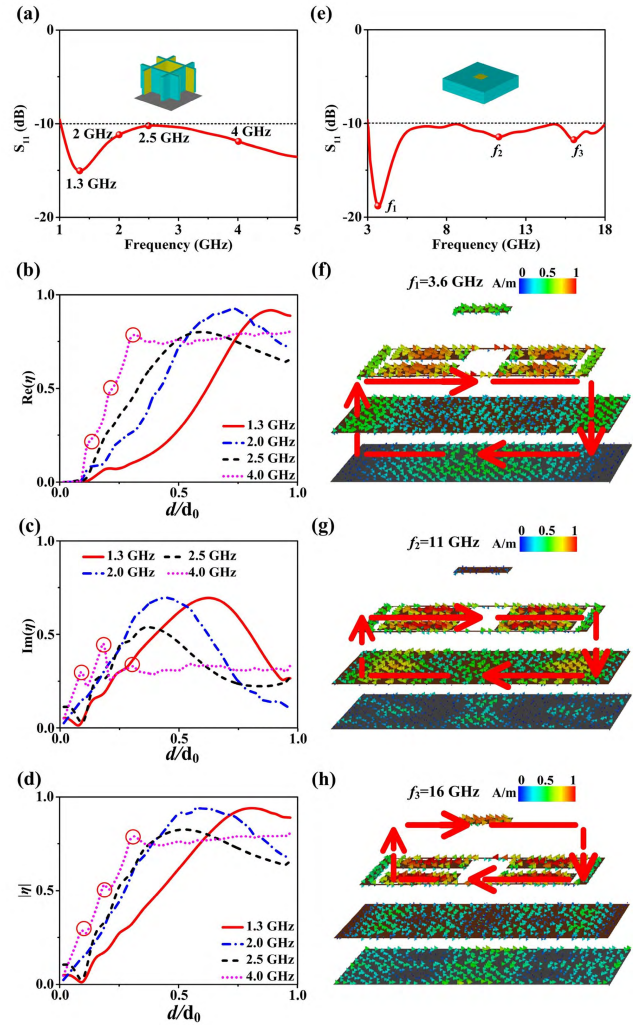


FIGURE 6. The retrieved wave impedance and current distributions at different frequencies. Simulated reflection coefficients for the (a) Huygens metasurface and (e) slab impedance metasurface. (b) Real part, (c) imaginary part and (d) amplitude of the wave impedance inside our structures. The current distributions at (f) 3.6 GHz, (g) 11 GHz and (h) 16 GHz, and the currents are normalized to the maximum value of currents at each frequency.

absorption band, the current distribution mode is illustrated in Fig. 6(h). Figs. 5(e) and 5(f) depict the absorption curves varying against the conductivity (σ_2) and side length of the ITO patch (l_1) on the top layer. We can see that the absorption ratio can be significantly enhanced as σ_2 decreases, while the operating frequency appears a blue shift with the increase of patch size. By carefully optimizing the structure parameters and the conductivity on each layer, we finally obtain an ultra-broadband absorption with very high efficiency. As shown in Fig. 4(b), the bandwidth of absorption ratio larger than 90% covers the range of 1 GHz to 18 GHz.

Then we retrieve the wave impedance inside the Huygens metasurface and the current distributions at three resonant frequencies to illustrate the mixed absorption mechanisms. Figs. 6(b-d) plot how the wave impedance changes inside our absorption structure at four typical frequencies (with the reflection coefficient shown in Fig. 6(a)), which is shined

by normally incident EM waves with an x polarization at low frequency range. The wave impedance η is estimated by the ratio of electric field \vec{E} and magnetic field \vec{H} , with the fields obtained by integrating over the xy plane at different positions within a meta-atom. Indeed, the designed Huygens metasurface can perfectly match the impedance ($\eta_0 = 377\Omega$) at the air/metasurface interface and the impedance curves change gently within the structure, which show great agreements with the theoretical prediction presented in Fig. 2(b). Meanwhile at frequencies with poor absorption, as in the range of 2-3 GHz, the wave impedance at the interface does not strictly match that of free space. In addition, at the transition frequencies, such as 4 GHz, the impedance curves exhibit some sharp peaks, which coincide well with that of the resonant structures (red curves shown in Fig. 2(b)). Figs. 6(f-h) plot the current distributions at three representative frequencies shown in Fig. 6(e). Different current distributions induce different magnetic resonances as expected, which broaden the working bandwidth at high frequency range. Referring to Fig. 6(f), the calculated current distributions at 3.6 GHz reveal that the magnetic resonance is due to the interaction between the two middle ITO structures and the continuous metallic layer. While the second magnetic resonance at 11 GHz is mainly generated by the mutual interaction between two middle ITO layers, as the current distribution shown in Fig. 6(g). The anti-parallel currents at 16 GHz are excited to flow on the upper two ITO layers, observed in Fig. 6(h). It is very obvious that we can easily get ultra-broadband absorption with high-efficiency via tuning the Huygens metasurface and the three-layers slab impedance metasurface.

III. EXPERIMENTAL RESULTS AND DISCUSSIONS

With the carefully optimized meta-atom in hand, we design/fabricate a microwave absorber sample (with a size of 600 mm \times 600 mm) consisting of a periodic array of typical meta-atoms. Figs. 7(a-c) present the photographs of the Huygens metasurface, slab impedance metasurface and the whole absorption sample. The upper Huygens metasurface is assembled by 60 zigzag-shape FR4 stripes (with a thickness of 2.5 mm) covered by ITO films, while for the slab impedance metasurface, three-layers of ITO patterns and FR4 layers are pasted together.

Next, we experimentally characterize the absorption performances of the sample by using three steps. In the first step, we measure the reflection coefficients of the Huygens metasurface by comparing the scattering property of our metasurface and that of the metal slab with the same size. In our experiment, two broad band horn antennas are connected to an Anritsu MS4644A vector analyzer to record the electronic filed information. Fig. 7(d) depicts the measured reflection coefficients and FDTD simulated results. Here, we should mention that the conductivity of ITO is chosen as 2×10^5 S/m for fabrication convenience. We can see clearly that the simulation results can perfectly reproduce all salient features of the experimental results. The best reflection appears at 1.2 (1.1) GHz for measurements (simulations).

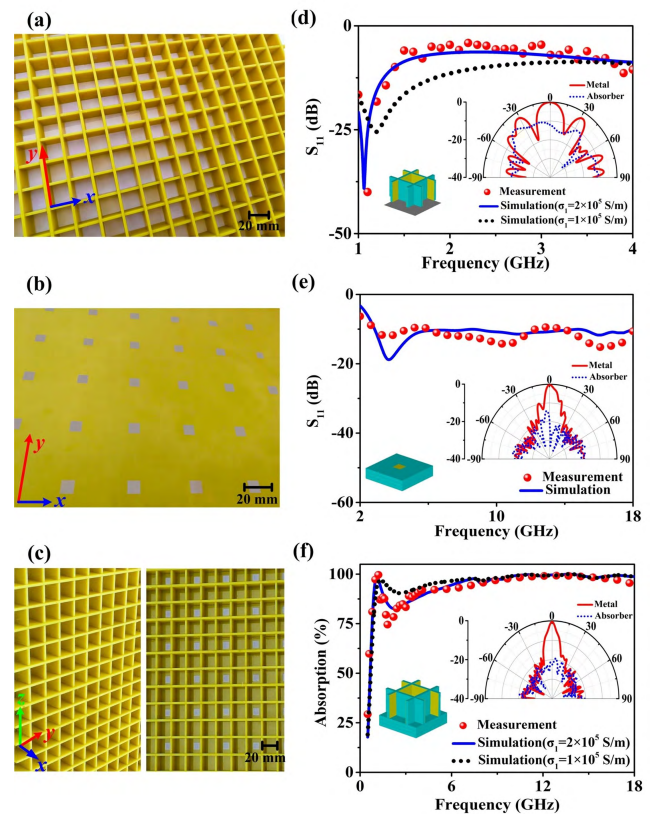


FIGURE 7. Performances of the fabricated absorber. Photographs of (a) fabricated Huygens metasurface, (b) slab impedance metasurface and (c) the whole sample. Simulated and measured reflection coefficients for (d) Huygens metasurface and (e) slab impedance metasurface. (f) Simulated and measured absorption efficiency of our designed absorber sample. Inset shows the measured far-field patterns at (d) 1.3 GHz, (e) 11 GHz and (f) 16 GHz for our absorber and the metallic slab with the same size of our structure.

And the reflection can be further decreased as $\sigma_1 = 1 \times 10^5$ S/m (with the -10 dB bandwidth covering 1-3 GHz), as demonstrated by the black dash line in Fig. 7(d). In the second step, we measure the reflection performance of the slab impedance metasurface by using the same approach with that of the Huygens metasurface. The reflection coefficients shown in Fig. 7(e), ordered by less than -10 dB, is from 2.9 GHz to 18 GHz for experimental results, while is from 3 GHz to 18 GHz for simulations. The slight difference is mainly attributed to the imperfections of the incoming wave fronts generated by our microwave horns and inevitable fabrication errors. We also note that three resonances appear at 3.6 GHz, 10.7 GHz and 16 GHz for the measurements. In the third step, we test the absorption efficiency of the complete fabricated sample. The Huygens metasurface and the slab impedance metasurface are assembled together by means of dielectric screws. Fig. 7(f) depicts the absorption ratio against frequency. We could find from simulation that the bandwidth of absorption rate exceeding 90% is from 1 GHz to 18 GHz ($\sigma_1 = 1 \times 10^5$ S/m). When we tune the conductivity of Huygens metasurface as $\sigma_1 = 2 \times 10^5$ S/m, the experimental absorption decreases to 75% at frequency of 2.65 GHz,

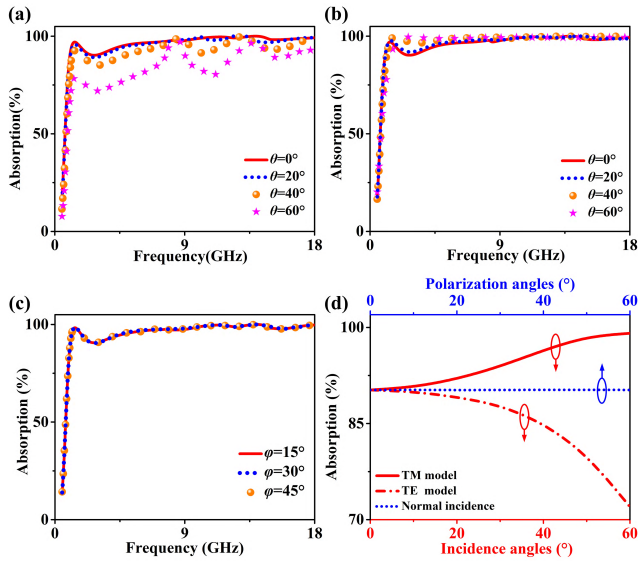


FIGURE 8. Absorber performances under oblique incidences and different polarizations. Simulated absorption ratios of the proposed absorber under different incident angles for (a) TE mode and (b) TM mode. (c) Simulated absorption rate of the proposed absorber under different polarizations. (d) Absorption ratios under different incident angles and polarizations.

and the simulation shows good agreement with the measurement. Moreover, the absorption at low frequency range and high frequency range affects each other due to the mutual coupling of near fields, resulting in a higher absorption rate in both frequency ranges. Here, we should note that the incident power is almost fully absorbed by our absorber, rather than scattered to other directions [35]–[38], this is evidenced by the far-field patterns shown insets of Figs. 7(d-f).

Finally, we discuss the absorption performance under oblique incidence and different polarizations. Because our absorber sample has a finite size, the absorption performance deteriorates strongly under oblique incidence, and we show these characteristics by FDTD simulations. Figs. 8(a) and 8(b) illustrate the absorption performances of the proposed absorber under conditions of oblique incidence for transverse electric (TE) wave and transverse magnetic (TM) wave, respectively. We note obviously that the absorption performances are quite different for TE and TM cases. It is because that the effective wave impedances η_{eff} changing against the incident angles for TM and TE waves are different. η_{eff-TM} decreases as the incident angles increases, whereas η_{eff-TE} varies oppositely, which can be expressed by the following equations,

$$\begin{aligned} \eta_{eff-TM} &= \eta \cos \theta \\ \eta_{eff-TE} &= \frac{\eta}{\cos \theta} \end{aligned} \quad (2)$$

However, our absorber is robust for incident angles varying $\pm 30^\circ$. The absorption efficiencies, defined as the least one at frequencies of 1-18 GHz for TE and TM waves, are plotted against incident angles in Fig. 8(d). The absorption rate can reach nearly 100% under TM incidence with $\theta = 60^\circ$, while

it decreases to 72% for TE incidence. The absorption difference can be attributed to the varied impedances as shown in Eq. (2). Fig. 8(c) illustrates different absorption rates under three representative polarization angles. We can obtain that our absorber is insensitive to polarizations due to the mirror symmetry along two polarization axes, which is very useful to apply in realistic system design.

IV. CONCLUSION

In summary, we propose an ultra-broadband microwave absorber via combining the Huygens metasurface and the slab impedance metasurface. The operating frequencies and absorption rates can be controlled by the structure size and conductivity, respectively. Numerical and experimental results have demonstrated that the absorption efficiencies can reach more than 90% within a large frequency interval (1 GHz to 18 GHz). In addition, our absorber is insensitive to oblique incidences and polarizations. Our absorber will be a good candidate for wide application to military and stealth techniques. Our discovery can stimulate other ultra-broadband meta-devices with high performances or absorber working at other frequency domains.

ACKNOWLEDGMENT

(Can-Yu Wang and Tong Cai contributed equally to this work.)

REFERENCES

- [1] K. Iwaszczuk, A. C. Strikwerda, K. Fan, X. Zhang, R. D. Averitt, and P. U. Jepsen, "Flexible metamaterial absorbers for stealth applications at terahertz frequencies," *Opt. Express*, vol. 20, no. 1, pp. 635–643, Dec. 2011.
- [2] J.-R. J. Gau, W. D. Burnside, and M. Gilreath, "Chebyshev multilevel absorber design concept," *IEEE Trans. Antennas Propag.*, vol. 45, no. 8, pp. 1286–1293, Aug. 1997.
- [3] E. Michielssen, J. M. Sajer, S. Ranjithan, and R. Mittra, "Design of lightweight, broad-band microwave absorbers using genetic algorithms," *IEEE Trans. Microw. Theory Techn.*, vol. 41, no. 6, pp. 1024–1031, Jun. 1993.
- [4] N. Yu et al., "Light propagation with phase discontinuities: Generalized laws of reflection and refraction," *Science*, vol. 334, no. 6054, pp. 333–337, Oct. 2011.
- [5] D. Schurig et al., "Metamaterial electromagnetic cloak at microwave frequencies," *Science*, vol. 314, no. 5801, pp. 977–980, Oct. 2006.
- [6] R. Liu, C. Ji, J. J. Mock, J. Y. Chin, T. J. Cui, and D. R. Smith, "Broadband ground-plane cloak," *Science*, vol. 323, no. 5912, pp. 366–369, Jan. 2009.
- [7] T. Cai et al., "High-efficiency and full-space manipulation of electromagnetic wave fronts with metasurfaces," *Phys. Rev. Appl.*, vol. 8, no. 3, 2017, Art. no. 034033.
- [8] T. Cai et al., "High-performance bifunctional metasurfaces in transmission and reflection geometries," *Adv. Opt. Mater.*, vol. 5, Nov. 2016, Art. no. 1600506.
- [9] G. Zheng, H. Mühlenbernd, M. Kenney, G. Li, T. Zentgraf, and S. Zhang, "Metasurface holograms reaching 80% efficiency," *Nature Nanotechnol.*, vol. 10, no. 4, pp. 308–312, Feb. 2015.
- [10] L. Li et al., "Electromagnetic reprogrammable coding-metasurface holograms," *Nature Commun.*, vol. 8, no. 1, Aug. 2017, Art. no. 197.
- [11] F. F. Qin, Z. Z. Liu, Z. Zhang, Q. Zhang, and J. J. Xiao, "Broadband full-color multichannel hologram with geometric metasurface," *Opt. Express*, vol. 26, no. 9, pp. 11577–11586, Apr. 2018.
- [12] N. I. Landy, S. Sajuyigbe, J. J. Mock, D. R. Smith, and W. J. Padilla, "Perfect metamaterial absorber," *Phys. Rev. Lett.*, vol. 100, May 2008, Art. no. 207402.

- [13] Y. Ma, Q. Chen, J. Grant, S. C. Saha, A. Khalid, and D. R. S. Cumming, "A terahertz polarization insensitive dual band metamaterial absorber," *Opt. Lett.*, vol. 36, no. 6, pp. 945–947, Apr. 2011.
- [14] X. Shen *et al.*, "Triple-band terahertz metamaterial absorber: Design, experiment, and physical interpretation," *Appl. Phys. Lett.*, vol. 101, no. 15, 2012, Art. no. 154102.
- [15] X.-Y. Peng, B. Wang, S. Lai, D. H. Zhang, and J.-H. Teng, "Ultrathin multi-band planar metamaterial absorber based on standing wave resonances," *Opt. Express*, vol. 20, no. 25, pp. 27756–27765, Nov. 2012.
- [16] G. M. Akselrod *et al.*, "Large-area metasurface perfect absorbers from visible to near-infrared," *Adv. Mater.*, vol. 27, pp. 8028–8034, Dec. 2015.
- [17] K. Chaudhuri, M. Alhabeab, Z. Wang, V. M. Shalaev, Y. Gogotsi, and A. Boltasseva, "Highly broadband absorber using plasmonic titanium carbide (MXene)," *ACS Photon.*, vol. 5, pp. 1115–1122, Jan. 2018.
- [18] M. Luo, S. Shen, L. Zhou, S. Wu, Y. Zhou, and L. Chen, "Broadband, wide-angle, and polarization-independent metamaterial absorber for the visible regime," *Opt. Express*, vol. 25, no. 14, pp. 16715–16724, Jul. 2017.
- [19] Z. Yin *et al.*, "Electrically tunable terahertz dual-band metamaterial absorber based on a liquid crystal," *RSC Adv.*, vol. 8, pp. 4197–4203, Jan. 2018.
- [20] B.-X. Wang and G.-Z. Wang, "New type design of the triple-band and five-band metamaterial absorbers at terahertz frequency," *Plasmonics*, vol. 13, pp. 123–130, Jan. 2018.
- [21] Y. J. Kim *et al.*, "Ultrathin microwave metamaterial absorber utilizing embedded resistors," *J. Phys. D, Appl. Phys.*, vol. 50, no. 40, 2017, Art. no. 405110.
- [22] F. Ding, Y. Cui, X. Ge, Y. Jin, and S. He, "Ultra-broadband microwave metamaterial absorber," *Appl. Phys. Lett.*, vol. 100, no. 10, 2012, Art. no. 103506.
- [23] H. Xiong, Y.-B. Wu, J. Dong, M.-C. Tang, Y.-N. Jiang, and X.-P. Zeng, "Ultra-thin and broadband tunable metamaterial graphene absorber," *Opt. Express*, vol. 26, no. 2, pp. 1681–1688, Jan. 2018.
- [24] D. Ye *et al.*, "Ultrawideband dispersion control of a metamaterial surface for perfectly-matched-layer-like absorption," *Phys. Rev. Lett.*, vol. 111, no. 18, Oct. 2013, Art. no. 187402.
- [25] D. Lee, H. Jeong, and S. Lim, "Electronically switchable broadband metamaterial absorber," *Sci. Rep.*, vol. 7, Jul. 2017, Art. no. 4891.
- [26] M. Yoo and S. Lim, "Polarization-independent and ultrawideband metamaterial absorber using a hexagonal artificial impedance surface and a resistor-capacitor layer," *IEEE Trans. Antennas Propag.*, vol. 62, no. 5, pp. 2652–2658, May 2014.
- [27] M. Kenney, J. Grant, Y. D. Shah, I. Escorcía-Carranza, M. Humphreys, and D. R. S. Cumming, "Octave-spanning broadband absorption of terahertz light using metasurface fractal-cross absorbers," *ACS Photon.*, vol. 4, pp. 2604–2612, Sep. 2017.
- [28] C. Tresp, C. Zimmer, I. Mirgorodskiy, H. Gorniaczyk, A. Paris-Mandoki, and S. Hofferberth, "Single-photon absorber based on strongly interacting Rydberg atoms," *Phys. Rev. Lett.*, vol. 117, Nov. 2016, Art. no. 223001.
- [29] E. Galiffi, J. B. Pendry, and P. A. Huidobro, "Broadband tunable THz absorption with singular graphene metasurfaces," *ACS Nano*, vol. 12, pp. 1006–1013, Jan. 2018.
- [30] F. Ding, S. Zhong, and S. I. Bozhevolnyi, "Vanadium dioxide integrated metasurfaces with switchable functionalities at terahertz frequencies," *Adv. Opt. Mater.*, vol. 6, Feb. 2018, Art. no. 1701204.
- [31] W. Li, M. Chen, Z. Zeng, H. Jin, Y. Pei, and Z. Zhang, "Broadband composite radar absorbing structures with resistive frequency selective surface: Optimal design, manufacturing and characterization," *Compos. Sci. Technol.*, vol. 145, pp. 10–14, Jun. 2017.
- [32] C. Pfeiffer and A. Grbic, "Metamaterial Huygens' surfaces: Tailoring wave fronts with reflectionless sheets," *Phys. Rev. Lett.*, vol. 110, no. 19, May 2013, Art. no. 197401.
- [33] J.-P. Berenger, "A perfectly matched layer for the absorption of electromagnetic waves," *J. Comput. Phys.*, vol. 114, no. 2, pp. 185–200, 1994.
- [34] C. Qu *et al.*, "Tailor the functionalities of metasurfaces based on a complete phase diagram," *Phys. Rev. Lett.*, vol. 115, Dec. 2015, Art. no. 235503.
- [35] T. J. Cui, M. Q. Qi, X. Wan, J. Zhao, and Q. Cheng, "Coding metamaterials, digital metamaterials and programmable metamaterials," *Light Sci. Appl.*, vol. 3, Oct. 2014, Art. no. e218.
- [36] L.-H. Gao *et al.*, "Broadband diffusion of terahertz waves by multi-bit coding metasurfaces," *Light Sci. Appl.*, vol. 4, Sep. 2015, Art. no. e324.
- [37] J. Su *et al.*, "Ultra-wideband, wide angle and polarization-insensitive specular reflection reduction by metasurface based on parameter-adjustable meta-atoms," *Sci. Rep.*, vol. 7, Feb. 2017, Art. no. 42283.
- [38] Y. Zhuang, G. Wang, J. Liang, T. Cai, W. Guo, and Q. Zhang, "Flexible and polarization-controllable diffusion metasurface with optical transparency," *J. Phys. D, Appl. Phys.*, vol. 50, no. 46, 2017, Art. no. 465102.



CAN-YU WANG was born in China, in 1995. He received the B.S. degrees in electromagnetic field and microwave technology from the Air Force Engineering University, Xi'an, China, in 2017, where he is currently pursuing the M.S. degree.

His research interests include metamaterials, metasurfaces, and their applications to broadband perfect absorber.



JIAN-GANG LIANG was born in China, in 1975. He received the B.S., M.S., and Ph.D. degrees in electromagnetic field and microwave technology from the Air Force Engineering University, Xi'an, China, in 1997, 2000, and 2004, respectively, where he is currently the youngest Head of the Microwave Theory and Application Laboratory.

His research interests include microwave passive and active circuits, and antennas.



TONG CAI was born in China, in 1990. He received the B.S. and Ph.D. degrees in electromagnetic field and microwave technology from Air Force Engineering University, Xi'an, China, in 2012 and 2017, respectively.

His research interests include metamaterials, and metasurfaces and their applications to novel antennas and multifunctional devices. He has published over 10 peer-reviewed first-author papers in the *Advanced Optical Materials*, the *Physical Review Applied*, the *IEEE TRANSACTION ON ANTENNAS AND PROPAGATIONS*, the *Optics Express*, the *IEEE ANTENNAS AND WIRELESS PROPAGATION LETTERS*, the *Journal of Electromagnetic Waves and Applications*, the *Applied Physics A*, and the *Chinese Physics Letters*.

He has served as a Reviewer for the *IEEE ANTENNAS AND WIRELESS PROPAGATION LETTERS*, the *Journal of Electromagnetic Waves and Applications*, the *AEU International Journal of Electronics and Communications*, and the *IET Antennas and Wireless Propagations*.



HAI-PENG LI was born in China, in 1991. He received the B.S. and M.S. degrees in electromagnetic field and microwave technology from the Air Force Engineering University, Xi'an, China, in 2013 and 2015, respectively, where he is currently pursuing the Ph.D. degree.

His research interests include metamaterials, metasurfaces, and their applications to novel antennas and multifunctional devices. He has published over 10 peer-reviewed first-author papers in the *IEEE TRANSACTION ON ANTENNAS AND PROPAGATIONS*, the *IEEE ANTENNAS AND WIRELESS PROPAGATION LETTERS*, and the *Progress in Electromagnetic Research*.



WEN-YE JI was born in China, in 1994. He received the B.S. degrees in electromagnetic field and microwave technology from Air Force Engineering University, Xi'an, China, in 2017, where he is currently pursuing the Ph.D. degree.

His research interests include metamaterials, metasurfaces, and their applications to novel antennas and multifunctional devices.



CHENG-WU ZHANG was born in China, in 1981. He received the B.S. degree from the Nanjing University of Aeronautics and Astronautics, in 2005.

His research interests include performance of electromagnetic functional structure and design of stealth device.

• • •



QING ZHANG was born in China, in 1977. He received the B.S. degrees from the Shandong University of Electronic Engineering, in 2000. He is currently with The Aeronautical Science Key Lab for High Performance Electromagnetic Windows, Ji'nan.